Structure and electronic properties of Cu nanoclusters supported on $Mo_2C(001)$ and MoC(001) surfaces

Sergio Posada-Pérez,[a] Francesc Viñes,[a] José A. Rodríguez,[b] and Francesc Illas[a,*]

[a] *Departament de Química Física & Institut de Química Teòrica i Computacional (IQTCUB), Universitat de Barcelona, c/ Martí i Franquès 1, 08028 Barcelona, Spain.*

[b] *Chemistry Department, Brookhaven National Laboratory, Bldg. 555, Upton, NY 11973, USA.*

Abstract

The atomic structure and electronic properties of Cu_n nanoclusters (n = 4, 6, 7, and 10) supported on cubic nonpolar δ-MoC(001) and orthorhombic C- or Mo-terminated polar β-Mo_2C(001) surfaces have been investigated by means of periodic density functional theory based calculations. The electronic properties have been analyzed by means of the density of states, Bader charges, and electron localization function plots. The Cu nanoparticles supported on β-Mo_2C(001), either Mo- or C-terminated, tend to present a two-dimensional structure whereas a three-dimensional geometry is preferred when supported on δ-MoC (001), indicating that the Mo:C ratio and the surface polarity play a key role determining the structure of supported clusters. Nevertheless, calculations also reveal important differences between the C- or Mo-terminated β-Mo_2C(001) supports to the point that supported Cu particles exhibit different charge state, which opens a way to control the reactivity of these potential catalysts.

*Corresponding author: francesc.illas@ub.edu

Keywords: Density functional calculations • Molybdenum Carbide surfaces • Copper clusters • Charge transfer • Electronic structure

1. Introduction

Transition Metal Carbides (TMCs) are technological relevant materials with interesting physical properties such as extreme hardness,[1] excellent electric and thermal conductivities,[2] and high melting points.[3] These materials also exhibit remarkable chemical properties, especially in catalysis, where the pioneering work of Levy and Boudart provided evidence that, for a variety of reactions, the catalytic activity of WC was similar or even better than that of Platinum.[4] Compared to expensive late transition metals, TMCs are abundant, relatively cheap, and apparently tend to exhibit smaller activation energy barriers.[5] Since the work of Levy and Boudart, the number of reactions catalyzed by TMCs has greatly increased.[6-8] In addition TMCs are increasingly used as supports in catalysis[9] and electrocatalysis.[10] Following the initial work of Ono and Roldán-Cuenya on the catalytic activity of Au/TiC towards low temperature CO oxidation,[11] Rodríguez *et al*. have shown that Au nanoparticles deposited on TiC(001) are active towards adsorption and decomposition of SO_2 thus providing excellent catalysts for hydrodesulfurization.[12-16] Also, Au/TiC(001) systems have been found to catalyze H_2 and O_2 dissociation[17,18] indicating that these new family of catalysts may be appropriate for hydrogenation and oxidation reactions, the former being particularly of interest since avoids the formation of oxycarbides, with a concomitant degradation of the catalyst support. The formation of oxycarbides constitutes a common problem when atomic oxygen or some O-containing species interact with the surface of TMCs.[19-22]

In recent times, Au/TiC systems have been shown to perform extraordinarily well in the low temperature water gas shift reaction[23] and to provide active sites for CO_2 hydrogenation to methanol.[24,25] Regarding catalyzed CO_2 conversion to methanol, joint experimental and theoretical work indicated that CO_2 adsorption energy appears to be a good reactivity descriptor since it nicely follows the trend β-Mo_2C > δ-MoC > TiC >> Cu. Furthermore, CO_2 is strongly adsorbed on Cu and Au clusters supported on TiC and here adsorption energy also correlates with the methanol formation rate Cu/TiC(001) > Au/TiC(001) > Cu/ZnO(001) >> Cu(111).8 Thus, small Cu and Au clusters supported on TMCs are likely to provide potential alternative catalysts for methanol synthesis, in principle dozens of times better than the commercial Cu/ZnO based one, and there is already evidence that Cu/TiC provides excellent results for CO_2 to methanol catalytic

synthesis.[24,25] However, the choice of the best TMC support remains unknown. Here, it is worth mentioning that molybdenum carbides with MoC or Mo_2C stoichiometry display an interesting reactivity towards CO and CO_2 and have been used to study synthetic and reactive aspects associated to environmental processes.[26-28] In order to avoid any possible misunderstanding arising from the different notations used to denote the different phases of MoC and Mo_2C, it is worth pointing out that here we follow the notation convention defined by the Joint Committee on Power Diffraction Standards (JCPDS) data files,[29] as other authors did previously,[30] in which hexagonal and orthorhombic Mo_2C are denoted α-Mo_2C and β-Mo_2C, respectively. Note, however, that some authors in the literature refer to orthorhombic Mo_2C as α-Mo_2C,[31-33] following an early definition by Christensen.[34] In the case of MoC, the cubic phase is always referred to as δ-MoC.

Going back to the reactivity of MoC and Mo_2C, we note that the Mo terminated (001) surface of orthorhombic Mo_2C, hereafter denoted as β-Mo_2C(001)-Mo, has been theoretically and experimentally proposed for CO dissociation[35] and direct CO_2 conversion to methanol,[36,37] given that such a polar single crystal surface is easily achievable, and that it can easily capture, activate, and dissociate CO_2.[36] Likewise, β-Mo_2C has been recently found to be not only a good support to Ni nanoparticles, but also an active phase to the so-called Ni/β-Mo_2C bifunctional catalyst, used in methane dry reforming processes.[31,38-39] Furthermore, it has been predicted that δ-MoC(001) can easily dissociate molecular oxygen[22] and Density Functional Theory (DFT) based calculations showed the very high catalytic power of hexagonal α-Mo_2C on ammonia dehydrogenation.[26] Also, hexagonal α-Mo_2C(001) and orthorhombic β-Mo_2C phases have been considered as catalyst for CO hydrogenation.[30,32,40]

The preceding discussion strongly suggests that Cu nanoclusters supported on molybdenum carbides can exhibit enhanced reactivity towards methanol synthesis from CO_2, and that both support and supported Cu nanoclusters can run intertwined during the methanol synthesis. As a first mandatory step to investigate the chemical reactivity of these model catalysts, either from theory or experiments, information regarding the nature of the metal-support interaction and the structure of supported metal clusters is required. The present paper aims at providing this information through a systematic computational study

of Cu nanoclusters (hereafter referred to as Cu_n) deposited on β-Mo_2C(001)-Mo, β-Mo_2C(001)-C and δ-MoC(001) surfaces. The study is especially necessary in the case of β-Mo_2C surfaces since C and/or Mo terminations can be present in a single crystal or powder depending on the method followed for preparation and cleaning.[41,42] The paper is organized as follows. The second section defines the computational setup and presents the surface models. Next, the third section deals with the geometric and electronic structure of different Cu_n nanoclusters encompassing the two (*2D*) and three dimensional (*3D*) structures proposed by Jug *et al.*,[43] Jaque *et al.*,[44] as well as other possible structures dictated by the morphology of the underlying substrate. This is followed by the results for the Cu_n particles supported on the different surfaces. Finally, conclusions are drawn in the fourth section.

2. Surface models and computational details

The β-Mo_2C(001)-Mo, β-Mo_2C(001)-C, and δ-MoC(001) surfaces have been represented by appropriate slab models containing four atomic layers. Previous studies showed how structural and energetic properties varied below 5% by using thicker slabs.[45] A vacuum region superior to 10 Å in all cases is added in the direction perpendicular to the surface thus ensuring essentially no interaction between repeated slabs along the surface direction. In these slab models, the two outermost layers are fully relaxed where the bottom ones are kept at the bulk optimized geometry to provide an appropriate environment to the surface region. Whereas in both δ-MoC and β-Mo_2C a Mo→C electron density transfer exists, this charge unbalance remains essentially unaltered for δ-MoC(001) surface, but slightly strengthened on β-Mo_2C(001)-C yet mildly weakened in β-Mo_2C(001)-Mo one.[45] However, despite affecting the surface polarity, the effect on the estimated workfunctions is small, and the electronic structure was found to be rather similar for both polar surfaces. Note in passing by that β-Mo_2C (001) surfaces, despite being polar, display a reduced dipole moment, below 0.7 e·Å, which is consistent with the mixed ionic, covalent, and metallic character of the bonding.[45] Depending on the size of the Cu_n particle, (2×2) or (3×3) surface supercells have been employed.

The geometry of the naked surface models, gas phase Cu_n clusters, and the combination of both resulting in supported particles have been obtained from total energy minimization with the energy obtained from (periodic) DFT based calculations carried out

using the Vienna *Ab initio* Simulation Package (VASP).[46] Exchange-correlation effects have been accounted for by means of the generalized gradient approximation using the Perdew-Burke-Ernzerhof (PBE) exchange-correlation potential.[47] This approach has proven to provide an adequate description of MoC and Mo_2C bulk and surfaces[45] while providing a balanced description of the three series of transition metals.[48,49] Note that for TMCs, which display a strong metallic character in the vicinities of the Fermi energy level, the usage of hybrid functionals or other approaches suited for semiconductors or isolators is discouraged. In the present calculations, the valence electron density is expanded in a plane-wave basis set and the interactions between core and valence electrons described by the projector-augmented wave method of Blöchl[50] as implemented by Kresse and Joubert.[51] The kinetic energy cut-off for the plane wave basis set was set to 415 eV, proven to be enough to gain converged results for adsorbates on carbides in general, and in molybdenum carbides in particular. Integration in the reciprocal space was carried out by means of a 3×3×1 Monkhorst-Pack[52] scheme for cubic δ-MoC(001) nonpolar surfaces and a 5×5×1 grid for polar β-Mo_2C(001)-Mo and β-Mo_2C(001)-C surfaces in the case of (2×2) supercells. The use of (3×3) supercells involves an increase in the number of atoms and cell dimensions and, consequently, the number of **k**-points was reduced to **Γ**-point for cubic and orthorhombic surfaces. For the isolated Cu_n systems, calculations were carried out at the **Γ**-point. The convergence criterion for relaxation of atomic positions was adjusted so that all forces acting on atoms were always smaller than 0.01 eV $Å^{-1}$. The electronic relaxation was considered converged when the total energy in subsequent iterations varied less than 10^{-5} eV. For further information the interested reader is addressed to Ref. 45.

The cohesion energy (E_{coh}) of the gas phase Cu_n particles is defined as in Eq. (1)

$$E_{coh} = \frac{E_{Cu_n} - n\,E_{Cu}}{n} \qquad (1)$$

where E_{Cu_n} is the energy of a Cu_n isolated particle in an asymmetric box of 9×10×11 or 12×13×14 Å dimensions, depending on *n*, the number of Cu atoms in the particle; E_{Cu} is the energy of a single Cu atom. The adsorption energy, E_{ads}, of the Cu_n nanocluster has been calculated according to:

$$E_{ads} = E_{Cu_n/Mo_xC} - (E_{Mo_xC} + E_{Cu_n}) \qquad (2)$$

where E_{Cu_n/Mo_xC} is the energy of Cu_n adsorbed on the corresponding surface, E_{Cu_n} is the energy of the most stable isolated Cu_n nanoparticle for each cluster size, and E_{Mo_xC} is the energy of the Mo_xC pristine (001) surface where x= 1, 2 for δ-MoC and β-Mo_2C, respectively. The E_{ads}/atom was calculated as the adsorption energy value divided by the number of Cu atoms in the nanocluster. Starting from E_{ads} value, one can define the adhesion energy (E_{adh}) of the Cu_n on the Mo_xC surfaces as in Eq. 3

$$E_{adh} = E_{ads} - E_{def}^{surf} - E_{def}^{Cu_n} \quad (3)$$

where E_{def}^{surf} is the difference between the energy of the isolated surface at the relaxed equilibrium geometry and at the geometry adopted upon Cu_n adsorption, and $E_{def}^{Cu_n}$ is the energy difference for the isolated Cu_n particle at the optimum geometry at the surface and the one corresponding to the gas phase structure. The logic for the energy decomposition in Eq. (3) is sketched in Figure S1 in the supplemental material.[53] Eventually, in some cases, in order to compare different systems with the same number of atoms, the relative energy (E_{rel}) has been used, where the 0.00 energy value corresponds to the most stable gas phase structure whereas other values are the energy difference between a given structure and the most stable one.

Furthermore, in the case of ML systems, the degree of strain has been calculated as;

$$\frac{d_{Cu-Cu\,(ML)} - d_{Cu-Cu\,(Bulk)}}{d_{Cu-Cu\,(Bulk)}} \times 100 \quad (4)$$

where $d_{Cu-Cu\,(ML)}$ is the average between nearest-neighbor Cu-Cu distances on ML and $d_{Cu-Cu\,(Bulk)}$ is the Cu-Cu distance in bulk Cu —2.567 Å as predicted by the PBE functional.[48] Positive values indicate expansion whereas negative ones a compression process.

On the basis of absolute energy values, most favorable Cu_n/Mo_xC sytems have been further analyzed by means of Density of States (DOS), Electron Localization Function (ELF),[54] and Bader charge analysis.[55] DOS calculations have been performed using the tetrahedron method and the same convergence criteria and grid as in the optimization calculations, except for the (3×3) supercells, in which the number of used **k**-points is the same than (2×2) supercells in order to use the tetrahedron method. Cu isolated calculations

have been performed using the smearing method proposed by Methfessel-Paxton.

3. Results

3.1 Isolated clusters

In this section the study of isolated Cu nanoclusters is presented with emphasis on previous Cu_n structures proposed in the literature.[56-59] Several other candidate structures have also been considered on the basis of the analysis of different possible surface adsorption sites on each surface, of previous studies about Cu atoms supported on cubic δ-MoC(001),[60] and also of Cu nanoclusters supported on TiC(001).[61] The complete set of selected clusters considered in the present work is shown in Figure 1. The number of two-dimensional (2D) clusters is quite large despite the fact that for n>7 the three-dimensional (3D) structures are more stable.[56] The reasons for this choice comes from previous experimental work which indicates that, at small coverages, transition metal clusters supported on TMC tend to acquire planar structures.[13,23] This behavior results from the fact that metal-surface interactions are larger than metal-metal ones, favoring 2D supported clusters even if their gas phase counterparts are higher in energy than the 3D ones.[9,13,23]

Following these premises, different sizes and geometries of Cu_n clusters have been investigated with n= 4, 6, 7, and 10. In each case, the Cu-Cu distances are reported in the supplemental material[53] and, logically, these are smaller than the nearest-neighbor Cu-Cu distances in bulk Cu —of 2.567 Å as predicted by the PBE functional[48]— simply because of larger number of coordinately unsaturated atoms. The effect decreases as the number of atoms in the cluster increases. For the Cu_4 cluster several isomers are considered; these are a pair of 2D geometries— a square and a rhombus (Figures 1a,b)— and one 3D tetrahedron structure (Figure 1c). The results in Table 1 show that the rhombus structure is the most stable one, followed by square and tetrahedron structures and this is in agreement with previous calculations by Calaminici *et al.*[56] obtained at PW86x-P86c level. Next we consider the Cu_6 cluster since previous studies[43,44] show that this is the largest cluster where the most stable isomer is still planar (see Figure 1d). The present results are in full agreement with previous studies even if some Cu-Cu distances are slightly different, which can be attributed to the use of different functionals and basis sets. Also, 3D structures for Cu_6 clusters have been optimized; all of them were found to exhibit higher energy (> 0.8

eV) than 2D clusters. Furthermore, 3D clusters did not show similarities with the surface morphology, and consequently, they have not been taken into account as adsorption candidates. Regarding Cu_7 and Cu_{10}, we first considered the 3D geometries proposed by Jug *et al.*[43] (Figures 1e and 1h, respectively). Nevertheless, one needs to realize that, once adsorbed, the number of Cu-surface interactions is larger for other 3D or even 2D possible structures. For this reason, close-packed Cu_7 and Cu_{10} hexagonal (Figures 1f, 1g, 1i, and 1j) nanoclusters were included in the study despite the fact that these isomers are higher in energy (~ 1 eV) than those reported by Jug *et al.*[43] (Table 1). The structure of the close-packed clusters is in agreement with the results of Balbuena *et al.*[62] It is important to note that preliminary results show that isolated Cu atoms on β-Mo_2C(001)-Mo prefer hollow sites and, hence, Cu_7 and Cu_{10} hexagonal nanoclusters nicely fit above the hollow sites of the β-Mo_2C(001)-Mo surface.

Finally, to model very large flat supported Cu nanoparticles we consider a full monolayer with 16 Cu atoms in a close-packed arrangement above the appropriate supercell. For β-Mo_2C(001)-Mo surface with the (2×2) supercell there is 1:1 Cu:Mo relation whereas for the δ-MoC(001) surface also with a (2×2) supercell, this relation is 2:1, since the first layer of cubic surface contains eight C atoms and eight Mo atoms. Logically, the geometry of close-packed Cu_{16} overlayer was modified depending on the surface to, in each case, accommodate the cell parameters.

The DOS analysis of isolated Cu_n (Figure 2) presents discrete bands, as expected, and a broad peak at the Fermi level, which is a first indicative of conducting materials even if this can be biased by the broadening procedure used to obtain the DOS plots. The peaks at lower energy correspond to Cu(3*d*) related levels and evolve to a 3*d* like band. The peaks located above to Fermi level corresponds to *s* states, while the broad peak near the Fermi level (a mixture of *s* and *d* states) is related to the metal conduction band. In the case of Cu_4, the square structure (Figure 1c) presents occupied electronic states closer (~1 eV) to Fermi level than rhombus or tetrahedron structures (~1.5 eV). The DOS plot shown for Cu_6 exhibits similar features and the same occurs for the 3D Cu_7 and Cu_{10} clusters (Figures 1e and 1h) even if there are noteworthy differences with respect to the clusters reported in the literature. The close-packed Cu_{10} cluster (Figure 1i) presents a occupied electronic band close to Fermi level which is at variance to Cu_7 (Figure 1f) and could attributed to the

increased possibility of delocalize the electrons in the cluster plane. Finally, there are some differences between the number of occupied states near Fermi level for Cu_7 and Cu_{10} 3D clusters (Figures 1g and 1j). Anyway, it is important to point out that these clusters are in the so-called non-scalable regime, *i.e* where every atom counts, and so distant from the scalable regime, where metallic delocalization is achieved.[63,64]

3.2 Supported clusters

The naked clusters describe in the previous section have next been deposited on the different Mo_nC (001) surfaces and the geometry fully optimized to take into account possible structural changes induced by interactions with the support. Moreover diverse adsorption sites were considered and overall more than 80 geometries have been investigated. Nevertheless, results in the next subsection correspond to the most stable cases.

3.2.1 Cu_n clusters supported on δ-MoC(001)

The study of the structure and electronic properties of Cu_4 supported on δ-MoC(001) has been carried out using the (2×2) supercell model. This supercell has also been used to investigate the case of a full Cu ML composed by 16 Cu atoms which provides a model for very large flat supported clusters. To avoid possible Cu-Cu interactions between in the periodically repeated images a (3×3) supercell has been used to mode adsorption of Cu_6 and Cu_7.

In the case of the supported Cu_4 cluster, the optimization procedure leads to two degenerate structures (Table 2). These are the tetrahedron and distorted rhombus displayed in Figures 3a and 3b. Upon interaction with the surface, the Cu_4 square nanocluster does not maintain its structure and evolves to distorted rhombus. Despite the fact that tetrahedron and rhombus structure are degenerate, the adsorption energy *per* atom is larger in the case of the tetrahedron because the naked cluster is higher in energy. In the Cu_4/MoC(001) system, the adhesion energy does not significantly differ from the adsorption energy implying that the surface and cluster deformation are not dominant. In the case of supported Cu_6 two degenerate structures are found as in the case of Cu_4 supported clusters; one of these corresponds to a 2D cluster which has a hexagon like shape (Figure 3c) whilst the other isomer corresponds to a 3D structure with a distorted rhombus in the first atomic

layer, which is reminiscent of the structure of the supported Cu_4 cluster, and two Cu atoms above these ones as seen in Figure 3d. Finally, regarding the structure of the supported Cu_7 cluster, a 3D structure is obtained, but significantly different from the Cu_7 isolated geometry predicted in the present work and also by Jug *et al.*[43] In fact, the structure of the supported cluster involved five Cu atoms adsorbed located not always above high symmetry adsorption sites, and two atoms forming the second layer (Figure 3e).

Let us now consider the case of full monolayer featuring a very large flat supported particle. The optimization of the supported Cu monolayer places the metal atoms on top of surface atoms as one can observe in Figure 3f, this is at variance of the case of single atoms tending to occupy MMC sites.[60] Interestingly, the structure of the supported monolayer exhibits a considerable rumpling essentially with eight Cu atoms on each layer. This follows from the different atomic radii of C and Mo with concomitant C-Cu distances (~1.97 Å) shorter than Cu-Mo (~3.30 Å). Once the most stable Cu monolayer supported on MoC(001) has been obtained, a isolated ML optimization was carried out to obtain the energy of the unsupported monolayer, which is necessary to estimate adsorption and adhesion energies, and the degree of strain, which indicates that the deposition of Cu ML brings down the compression respect the isolated Cu ML on δ-MoC(001) cell parameters — -3.14 and -8.13 %, respectively— (see Table S2), probably due to the fact that isolated ML is planar whereas deposited Cu ML becomes a bilayer, and consequenty, the strain decreases. With the aim of further investigating the possibility of existence of a stable planar monolayer additional calculations were performed using a Cu_8 planar cluster model formed by eight Cu single atoms placed above all possible high symmetry sites. In all cases, a 3D structure is obtained, which is in agreement with the trends discussed for supported Cu_6 and Cu_7 clusters, where planarity is not maintained. Taking into account the results mentioned above, one can argue that, except for very small clusters containing 3 or 4 atoms, the structure of supported Cu nanoparticles will tend to be 3D.

In order to gain additional information regarding the chemical interaction between the Cu clusters and the support we rely on the DOS plots reported in Figure 4, ELF plots in Figure S2 in the supplemental material,[53] and on net charges estimated from the Bader analysis. In the case of Cu_4/MoC(001), the DOS plots for the supported tetrahedron and rhombus structures do not exhibit significant variations and the same behavior is found for

the Cu_6 and Cu_7 supported particles. Apparently, the Cu *d* and *s* orbitals mix with the valence and conduction bands of the underlying carbide. The Bader analysis reveals a charge transfer from the metal cluster to the carbide surface as indicated by the ΔQ values in Table 2. Furthermore, the ELF plots in Figure 6 reveal a significant perturbation of the cluster electron density induced by the support. In the case of the Cu ML, the DOS analysis reveals that peaks arising from the Cu bilayer are closer to the Fermi level than in the case of the smaller particles, as expected from the larger degree of delocalization.

The Bader analysis shows that, in all obtained structures, there is charge transfer from the cluster to the carbide surface indicating that binding to the support tends to oxidize the metallic particle. In absolute terms, the largest transfer occurs for the Cu ML (Table 2), although the ΔQ *per* atom is larger for the Cu_4 clusters.

3.2.2 Cu_n clusters supported on β-Mo_2C(001)-Mo and β-Mo_2C(001)-C terminated surfaces

Here we concentrate on the structural and energetic stability of Cu nanoclusters supported on the β-Mo_2C(001)-Mo surface; the most salient results are summarized in Table 3. Similar to the case of Cu_4 on δ-MoC(001), the most stable Cu_4 structure correspond to a rhombus (see Figure 5a) with the Cu atoms above the Mo hollow sites. The large stability of this isomer is consistent with the fact that the majority of initial Cu_4 clusters converge to a rhombus, the next available stable structure being 1.2 eV higher in energy. It is worth pointing out that the different types of hollow Mo sites behave all in a similar way, the adsorption energy of the Cu_4 rhombus at these sites differ at most by 0.04 eV. Respect to Cu_7, the initial 3D cluster in Figure 1e becomes 2D upon interaction with the surface and the adsorption energy is nearly the same as for the final structure corresponding to the initial close-packed 2D isomer in Figure 1f. Hence, there is a clear trend to stabilize 2D structures as evidently seen in Figure 5b, which is a well-known fact since metal clusters tend to be planar, simulating a metal layer, in order to compensate the surface polarity.[65,66] This is also the case for the initial 3D close-packed cluster (Figure 1g) becoming more planar when supported on β-Mo_2C(001)-Mo (Figure 5c). A similar behavior is observed for the Cu_{10} clusters, the 3D cluster proposed in the literature (Figure 1h) evolves to a 2D structure (Figure 5e) and rearranges to an hexagonal structure. Nevertheless, the 2D close-packed structure from Figure 1i adsorbed on hollow Mo sites

presents a lower energy (Figure 5d) with a concomitant larger charge transfer from the surface to the supported particle, which may influence its catalytic activity. Moreover, the 3D hexagonal close-packed supported cluster (see Figure 5f) is higher in energy, as happened for isolated Cu_7.

From the obtained results one can conclude that Cu_4, Cu_7 or Cu_{10} nanoclusters supported on β-Mo_2C(001)-Mo follow the same pattern. This is in line with the analysis of the DOS plots in Figure 6 where the differences between supported clusters are almost indistinguishable. In comparison to the DOS plots for the isolated clusters, one can observe that, on average, Cu states are stabilized lying significantly below the Fermi Level. ELF plots in Figure S3 show all the same pattern. Interestingly, the Bader charge analysis shows that, contrarily to the case of Cu_n supported on the δ-MoC(001) surface, the charge transfer is from the β-Mo_2C(001)-Mo surface to the Cu nanoparticles. Hence, support effects imply a different chemistry, here the supported Cu nanoparticles become reduced.

Remarkably, the case of a Cu ML on β-Mo_2C(001)-Mo presents significant differences with respect to the structure supported on the δ-MoC(001) surface. First of all, the Cu ML deposited on β-Mo_2C(001)-Mo maintains a well-defined 2D geometry, thus following the trend observed for the smaller clusters. In all cases the Cu atoms are directly above hollow Mo sites (Figure 5g). Secondly, the adsorption energy *per* atom is similar to Cu_7 and slightly superior to Cu_{10} nanoclusters, which is not the case for the structures supported on the δ-MoC(001) surface, where Cu ML presents a adsorption energy *per* atom much smaller than the corresponding value for the supported Cu_4 clusters. Also, the DOS analysis shows that the dispersion of Cu states is slightly different depending of the support, since Cu ML on β-Mo_2C(001)-Mo features states higher in energy compared to Cu ML on δ-MoC(001). When Cu ML is adsorbed on β-Mo_2C(001) the Cu-Cu neighborhood distances are larger than Cu-Cu bulk and δ-MoC(001). Probably this fact is related with β-Mo_2C(001) cell parameter, which is larger than δ-MoC(001), and the adsorption site since Hollow Mo is the most reactive, but, the Mo-Mo distance on β-Mo_2C(001) surface is superior to Cu-Cu distance on bulk, and this fact provokes that Cu ML expands on both termination surfaces. When the isolated ML is optimized these Cu-Cu distances decrease and increase very slightly on β-Mo and β-C termination, respectively.

Moreover, as one can see in Figure 9d, the ELF plots are similar for Cu_7 and Cu_{10} nanoclusters whereas ELF plots on δ-MoC(001) surface showed a significantly lower on Cu atoms on monolayer.

In summary, Cu_n particles supported on orthorhombic β-Mo_2C(001)-Mo terminated exhibit decreasing adsorption energy *per* atom with increasing size as expected from the opposite trend in cohesive energy. Contrarily, the adhesion energy increases with cluster size. The most important and remarkable difference between the two supports (δ-MoC(001) or β-Mo_2C(001)-Mo) is on the sign of the charge transfer, Cu nanoparticles supported on the δ-MoC(001) surface tend to become oxidized whereas on β-Mo_2C(001)-Mo they are reduced. Another striking difference is on the structure of the supported particles, 3D particles are preferred on δ-MoC(001) whilst the 2D geometries are most favorable on the β-Mo_2C(001)-Mo surface, as commented above, owing to its polarity.

Results for Cu clusters supported on δ-MoC(001) and on β-Mo_2C(001)-Mo strongly suggest that surface polarity and/or Cu-C interaction play a key role determining the structure and oxidation state of the supported particles. To complete the study we also investigated the effect of the surface termination by considering the β-Mo_2C(001)-C terminated surface. This is also justified from the fact that experimental studies for β-Mo_2C are mostly carried out using powders exhibiting the two terminations.

As one can expect, the optimized geometries for the supported Cu_4, Cu_7, and Cu_{10} clusters correspond to a rhombus and to 2D close-packed structures, respectively (Figure 7). Moreover, in all cases, the Cu atoms occupy hollow Mo sites as in the case of the Mo terminated surface. The adsorption energy and adhesion energy values also follow the trend discussed for the Mo terminated surface; the corresponding results are summarized in Table 4. In the case of the Cu ML, the Cu atoms occupy the same sites as the smaller particles. The tendency to stabilize 2D structures is confirmed when realizing that, starting from the 3D Cu_{10} cluster proposed by Jug,[43] different stable 3D geometries are found for the supported particle but always more than 1 eV higher in energy that the 2D supported isomer. In this sense, both Mo and C terminations of polar β-Mo_2C(001), favors 2D supported clusters. Again, we note that this is at variance of the behavior reported above for Cu nanoparticles supported on the δ-MoC(001) surface. An interesting difference on the

effect of the β-Mo_2C(001) support on the electronic structure of the metallic particles concerns the charge transfer. In fact, results on Table 4 show that on β-Mo_2C(001)-C terminated the Cu particle tends to get oxidized as in the case of the δ-MoC(001) surface whereas on the β-Mo_2C(001)-Mo the particle gets reduce. This similarity points for a key role played by surface available C atom and polarity in the Cu_n oxidation process; when β-Mo_2C(001) is Mo terminated, the electron transfer is from Mo to C atoms, i.e. on the negative *z* axis direction, so Mo give electronic density to C atoms. Consequently, the dipole moment is along the positive *z* axis direction. The Cu_n deposition on Mo termination surface implies electron density charge transfer from Mo to Cu atoms, therefore, the charge transfer is on *z* axis direction, compensating the surface dipole. The opposite occurs on C-termination, but on the inverse direction. This opens an interesting way to tune the reactivity of the supported particles by support engineering. The DOS analysis (Figure 8) also follows the trend discussed for the systems presented above with remarkable electron delocalization showing up for the larger supported clusters. Regarding the ELF plots in Figure S4, one can see that C surface atoms interact strongly with Cu clusters with the formation of covalent like bonds.

Conclusions

Here a thorough systematic theoretical study has been presented regarding the atomic and electronic structure of Cu clusters supported on cubic δ-MoC and on orthorhombic β-Mo_2C-Mo and -C terminated (001) surfaces. Different Cu cluster sizes have been explored focusing on relative stability and particle morphology.

For the nonpolar δ-MoC(001) surface, small Cu_n clusters (n= 4, 6 and 7) and a Cu ML have been considered. The trends indicate that larger supported particles are likely to adopt a 3D structure and to become noticeable oxidized. This is confirmed by the Cu ML model featuring a rumpling bilayer structure being originated by Cu atoms located on top of surface C or Mo atoms.

For the polar β-Mo_2C(001)-Mo and -C surfaces, the results show that, in spite of the different termination, the supported particles tend to become 2D. However, the charge transfer direction is different for the two terminations in order to compensate the surface polarity. On the Mo terminated surface the supported particles tend to be reduced whereas

on the C terminated surface the supported particle tends to become oxidized. This difference may result in a different reactivity and suggests that it is possible to control the donor or acceptor character of the supported metallic particle by engineering the carbide support.

Acknowledgements

The research carried out at the *Universitat de Barcelona* was supported by the Spanish MINECO grant CTQ2012-30751 grant and, in part, by *Generalitat de Catalunya* (grants 2014SGR97 and XRQTC). This manuscript has been authored by employees of Brookhaven Science Associates, LLC under Contract No. **DE-SC0012704** with the U.S. Department of Energy. S.P.P. acknowledges financial support from Spanish MEC predoctoral grant associated to CTQ-2012-30751 and F.V. thanks the MINECO for a postdoctoral *Ramón y Cajal* (RyC) research contract (RYC-2012-10129). Computational time at the *MARENOSTRUM* supercomputer has been provided by the Barcelona Supercomputing Centre (BSC) through a grant from *Red Española de Supercomputación* (RES).

Table 1: Relative (E_{rel}) and cohesive (E_{coh}) energy (eV) of gas phase Cu_n nanoparticles of increasing size; structures are as in Figure 1.

N	**Structure**	**E_{rel}**	**E_{coh}**
4	Rhombus (1a)	0.00	-1.57
	Square (1c)	0.94	-1.37
	Tetrahedron (1b)	1.16	-1.28
6	2D (1d)[43]	0.00	-2.15
7	3D (1e)[43]	0.00	-2.05
	2D Close-packed (1f)	1.01	-1.91
	3D Close-packed (1g)	1.12	-1.89
10	3D[43] (1h)	0.00	-2.21
	2D Close-packed (1i)	0.84	-2.13
	3D Close packed (1j)	1.26	-2.09

Table 2: Relative energies (in eV), adsorption energy and adhesion energy *per* atom of Cu_n (n=4, 6, 7, ∞) supported on δ-MoC(001), the case with ∞ atoms is modeled by full monolayer. Charge transfer from the Bader analysis is reported as ΔQ, a positive charge implies that the supported cluster is oxidized. Information in parenthesis corresponds to the structures in Figure 1.

n	**Structure**	$\mathbf{E_{rel}}$	$\mathbf{E_{ads/atom}}$	$\mathbf{E_{adh/atom}}$	**ΔQ**
4	Tetrahedron (1b)	0.00	-1.35	-1.72	+0.42
	Rhombus (1a)	0.03	-1.35	-1.34	+0.47
6	2D (1d)[a]	0.00	-2.16	-2.47	+0.44
	3D (1d)[a]	0.08	-2.15	-2.42	+0.56
7	3D (1e)[a]	—	-1.91	-2.19	+0.79
∞	ML	—	-0.50	-0.51	+0.75

[a]Once supported on δ-MoC(001) these structures distort

Table 3: Relative energies (in eV), adsorption energy and adhesion energy *per* atom, and charge transfer (in a.u.) for the optimized structure of Cu_n supported on β-Mo_2C(001)-Mo. Information in parenthesis corresponds to the structures in Figure 1.

n	**Structure**	$\mathbf{E_{rel}}$	$\mathbf{E_{ads/atom}}$	$\mathbf{E_{adh/atom}}$	**ΔQ.**
4	Rhombus (1a)	—	-1.99	-2.24	-1.82
7	3D (1e)[43]	0.00	-1.55	-1.97	-2.19
	3D close-packed (1g)	1.42	-1.35	-1.76	-1.79
10	2D close-packed (1i)	0.00	-1.41	-1.81	-3.98
	3D (1h)[43]	0.39	-1.37	-1.76	-2.92
	3D close-packed (1j)	1.41	-1.27	-1.51	-2.03
∞	ML	—	-1.67	-1.73	-5.28

Table 4: Relative energies (in eV), adsorption energy and adhesion energy *per* atom, and charge transfer (in a.u.) for the optimized structure of Cu_n supported on β-Mo_2C(001)-C. Information in parenthesis corresponds to the structures in Figure 1.

n	**Structure**	$\mathbf{E_{ads/atom}}$	$\mathbf{E_{adh/atom}}$	**ΔQ**
4	Rhombus	-2.28	-2.71	+0.56
7	3D close-packed (1g)	-1.71	-2.52	+1.19
10	2D close-packed (1i)	-1.48	-2.42	+1.90
∞	ML	-1.66	-2.00	+1.99

Figure 1: Different structures and sizes of Cu nanoclusters selected. Geometries are shown in side views (top) and top views (bottom).

Cu_4			Cu_6
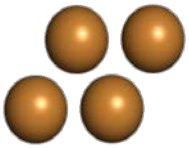	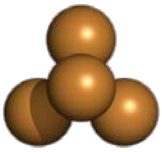		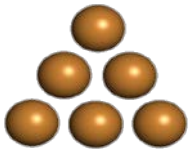
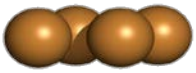	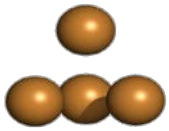	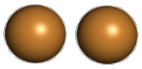	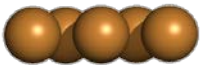
Rhombus (a)	Tetrahedron (b)	Square (c)	2D (d)

Cu_7		
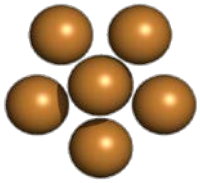	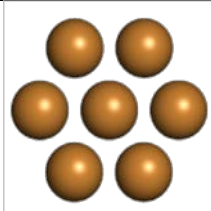	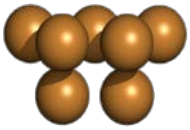
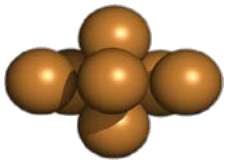	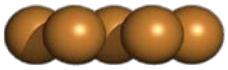	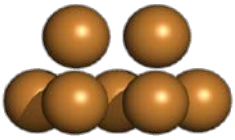
3D (e)[43]	Close packed 2D (f)	Close packed 3D (g)

Cu_{10}		
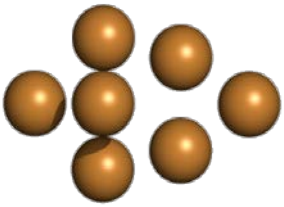	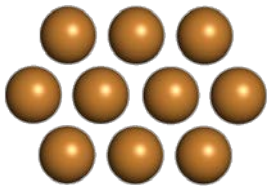	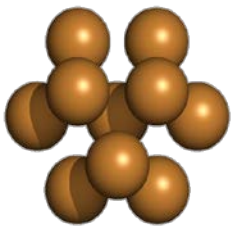
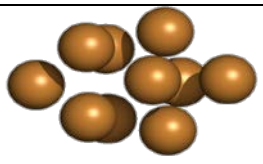	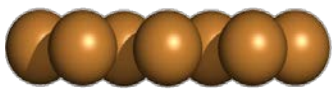	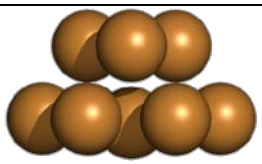
3D (h)[43]	Close packed 2D (i)	Close packed 3D (j)

Figure 2: Total DOS of isolated Cu nanoclusters. The notation is as in Figure 1. Different backgrounds correspond to different cluster sizes.

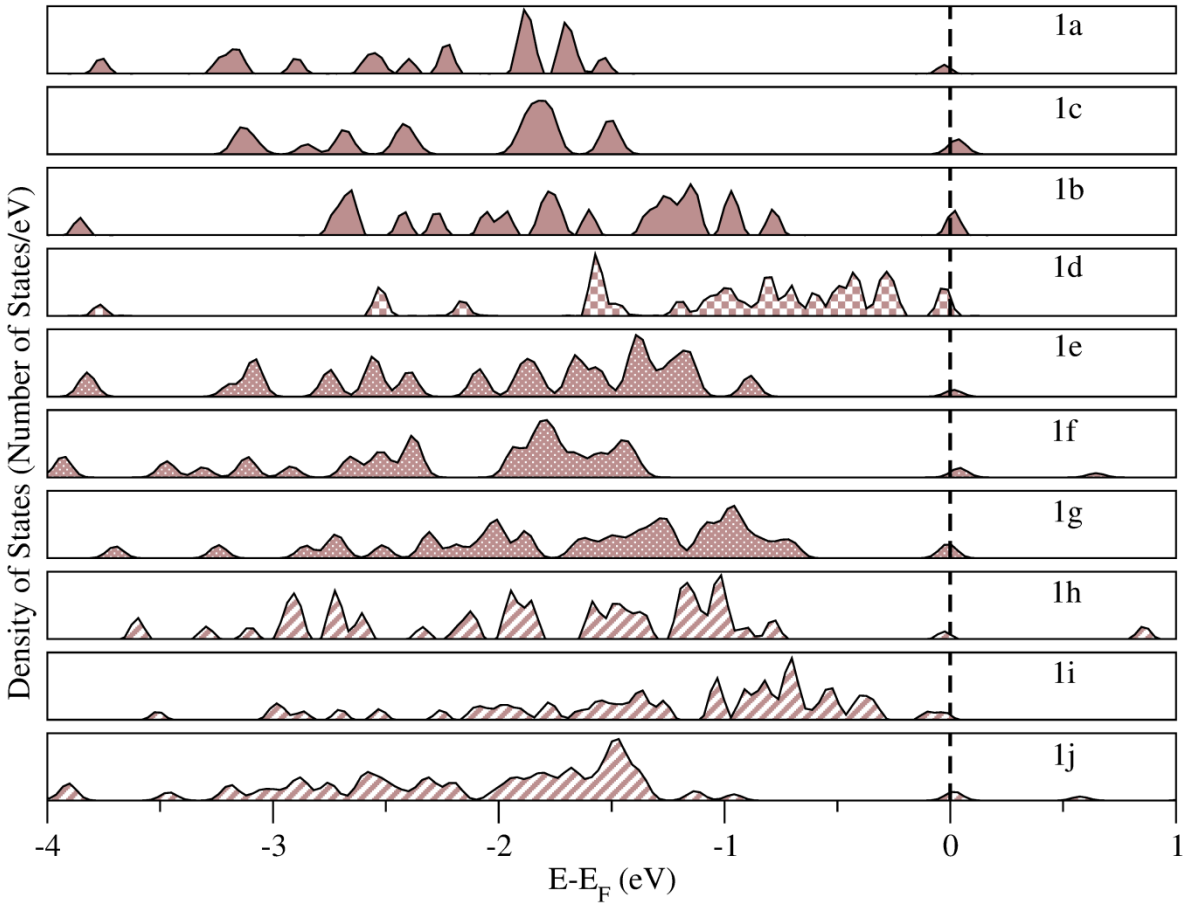

Figure 3: Top (upper panel) and side (bottom panel) views of the optimized structures of Cu_n supported on δ-MoC(001): Cu_4 tetrahedron (a), Cu_4 rhombus (b), Cu_6 2D (c), Cu_6 3D (d), Cu_7 3D (e), and Cu ML (f). Violet, green, and brown balls denote Mo, C and Cu atoms, respectively

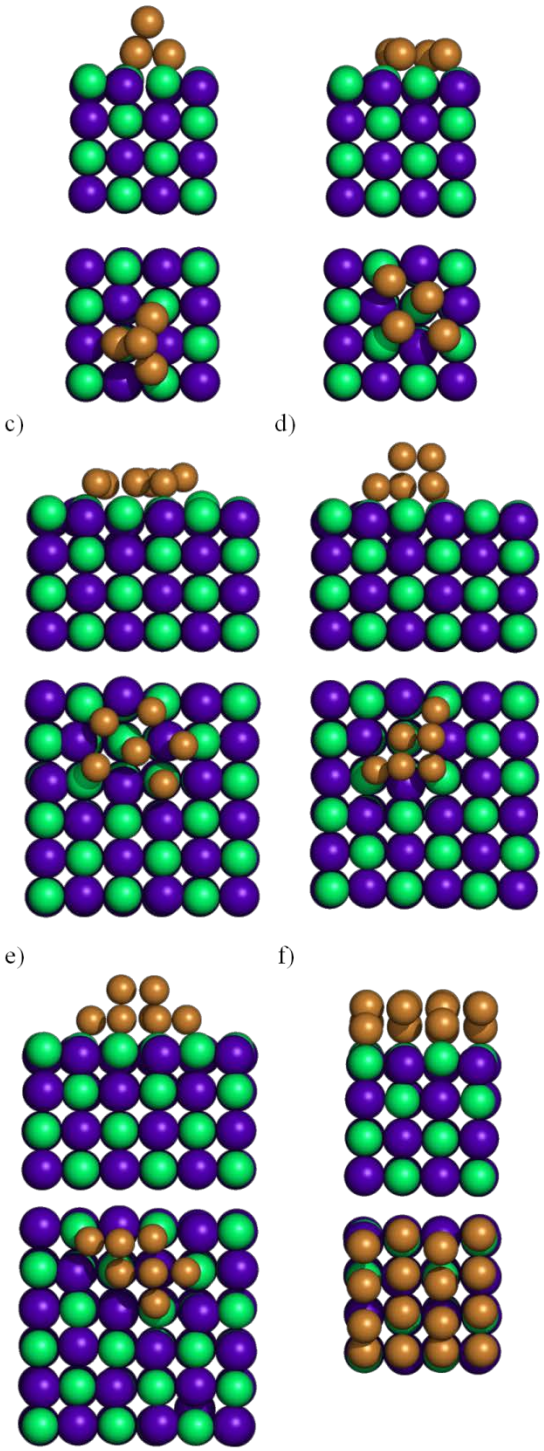

Figure 4: Total DOS of studied Cu nanoclusters adsorbed on δ-MoC(001). The *y* axis are not the same in the different graphs in order to facilitate the visualization.

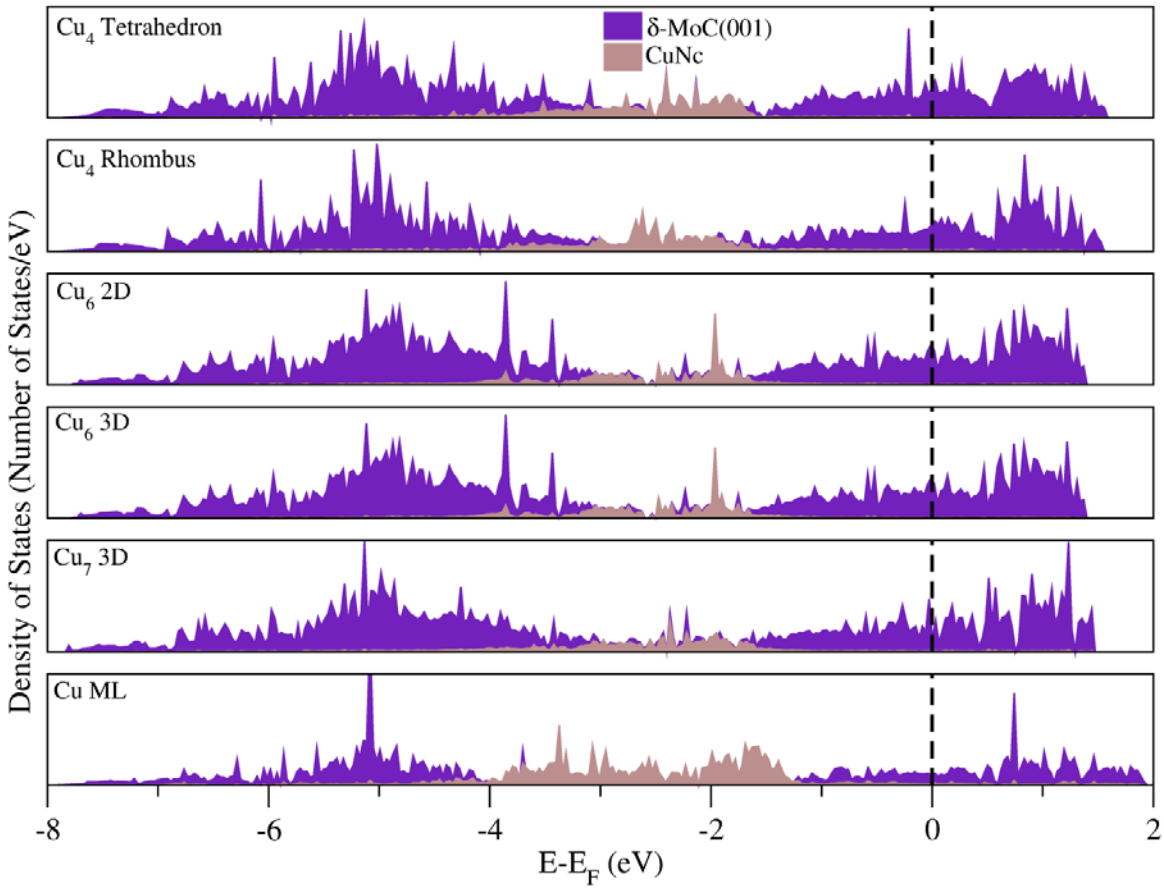

Figure 5: Structure of the Cu_n nanoparticles supported on the β-Mo_2C(001)-Mo surface: Cu_4 rhombus structure (a), Cu_7 2D close packed (b), Cu_7 3D close packed (c), Cu_{10} 2D close packed (d), Cu_{10} 3D become on 2D (e), Cu_{10} 3D close packed (f), and Cu ML (g). Side (top) and top views (bottom) are displayed. Sphere coloring as in Figure 3.

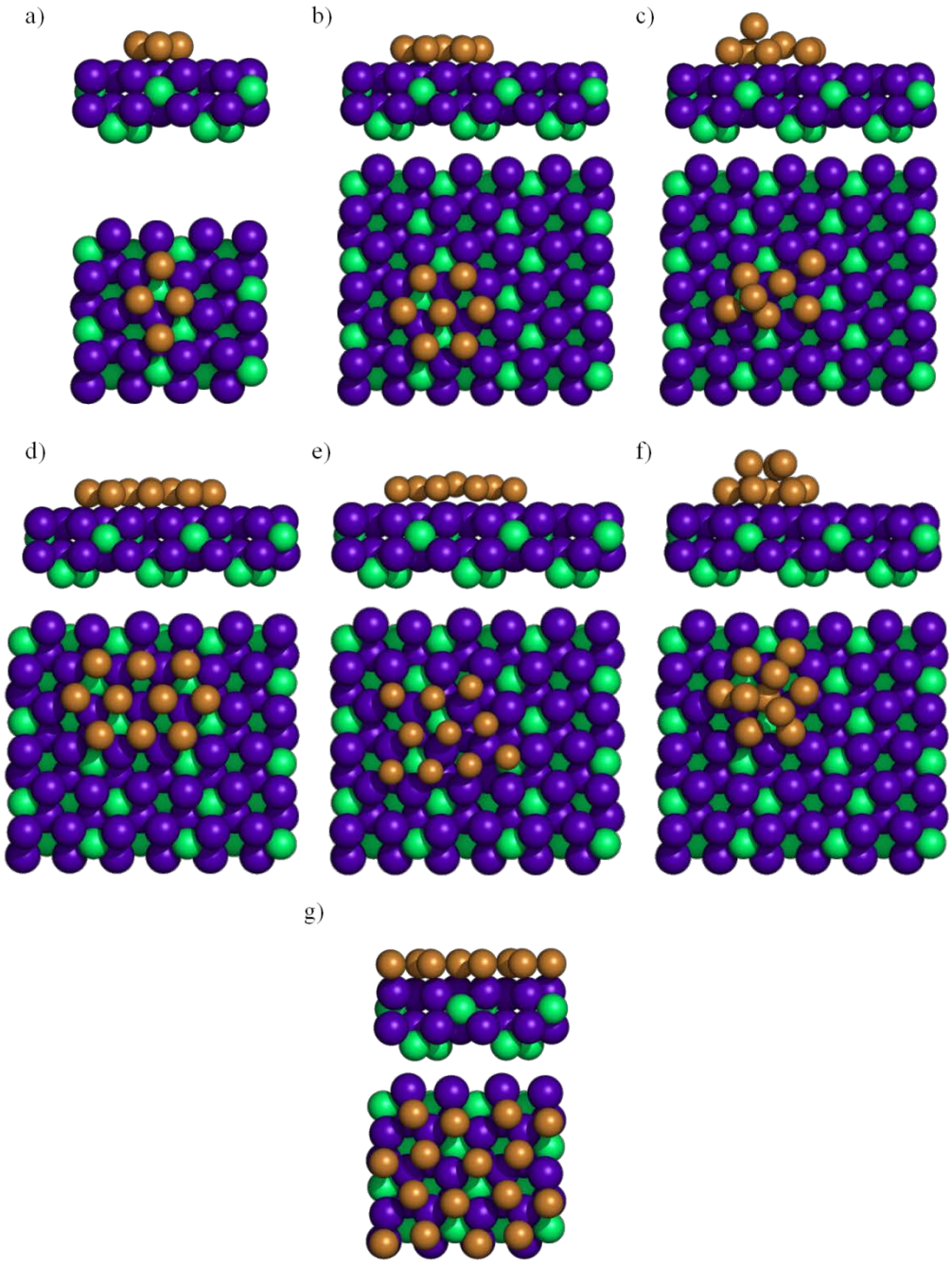

Figure 6: Total DOS of studied Cu nanoclusters adsorbed on β-Mo_2C(001)-Mo terminated. The *y* axis are not the same in the different graphs in order to facilitate the visualization.

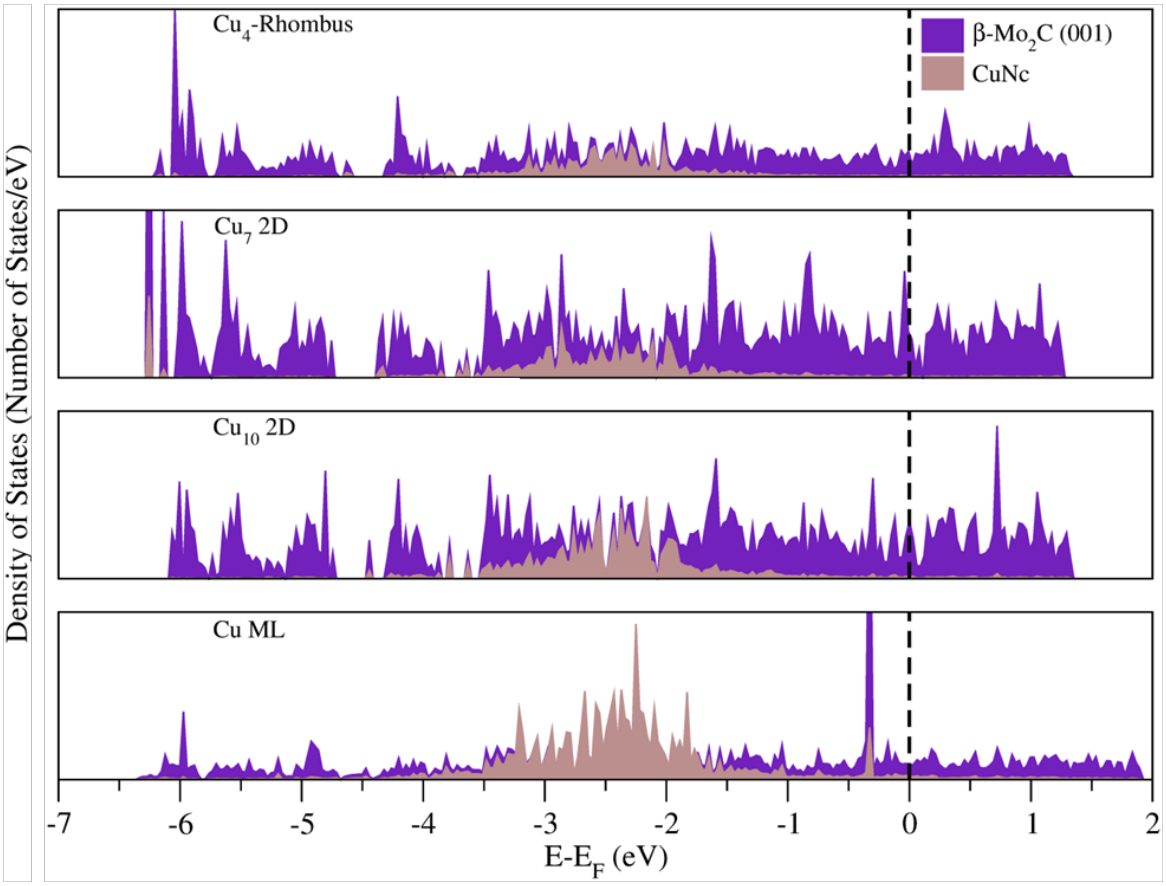

Figure 7: Sketches of the Cu_4 rhombus structure (a), Cu_7 (b), Cu_{10} (c), and Cu ML (d) deposited on β-Mo_2C(001)-C terminated. Side (top) and top views (bottom) are displayed. Sphere coloring as in Figure 3.

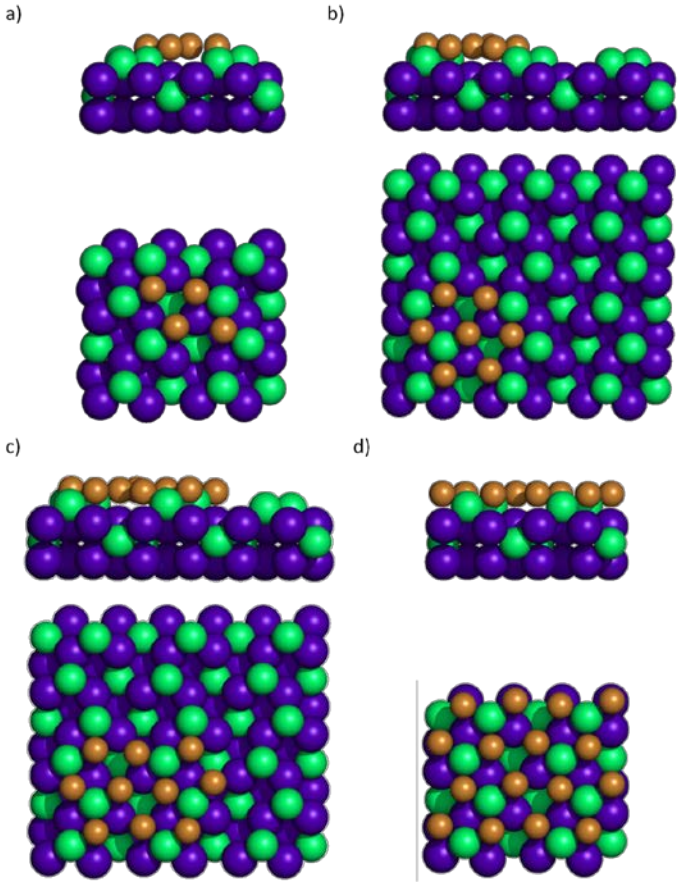

Figure 8: Total DOS of studied Cu nanoclusters adsorbed on β-Mo_2C(001)-C terminated. The *y* axis are not the same in the different graphs in order to facilitate the visualization.

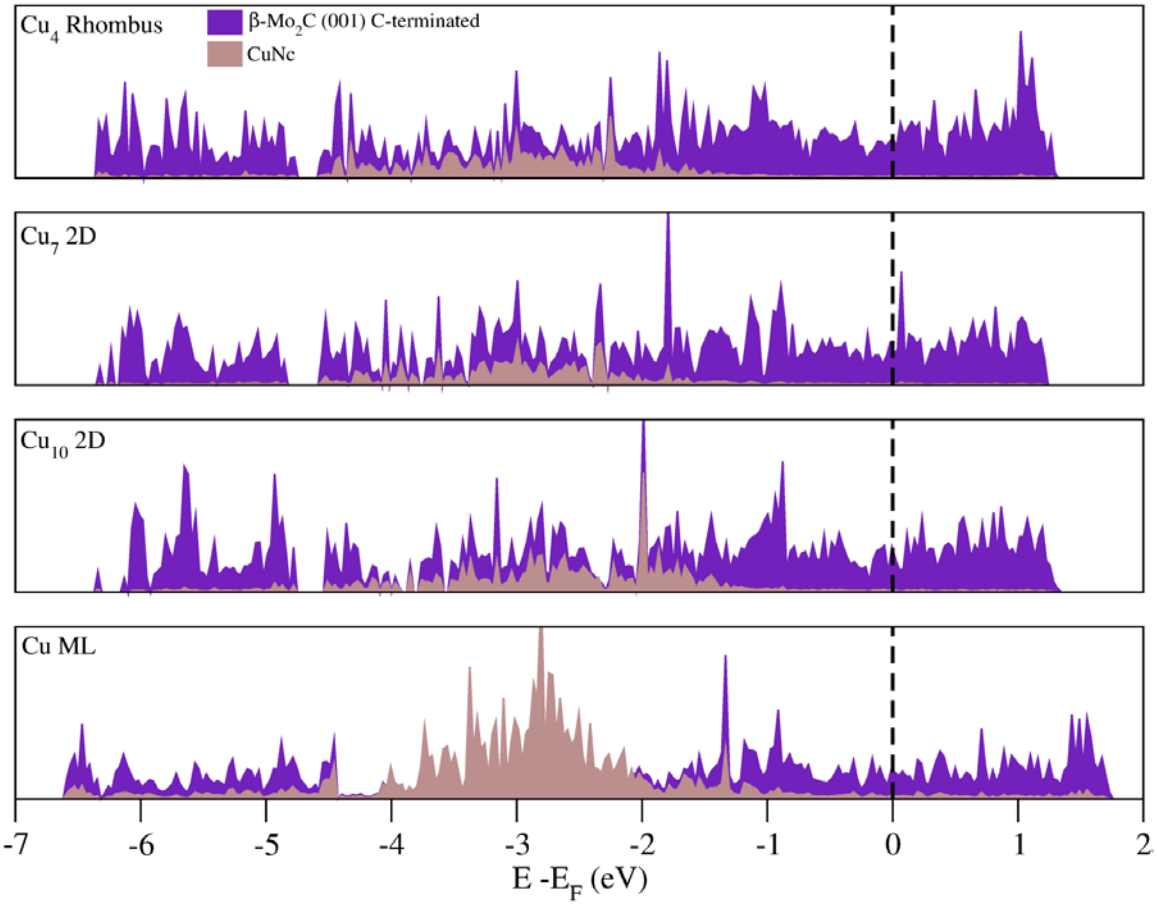

References

[1] J. J. Liao, R. C. Wilcox, and R. H. Zee, Scripta. Metall. Mater. **24**, 1647, (1990).

[2] H. H. Hwu and J. G. Chen, Chem. Rev. **105**, 185 (2005).

[3] J. A. Nelson and M. J. Wagner, Chem. Matter. **14**, 4460 (2002).

[4] R. B. Levy and M. Boudart, Science **181**, 547 (1973).

[5] F. Viñes, A. Vojvodic, F. Ablid-Pedersen, F. Illas, J. Phys. Chem. C **117**, 4168 (2013).

[6] H. C. Woo, K. Y. Park, Y. G. Kim, I. S. Nam, J. S. Chung, and J. S. Lee, Appl. Catal. **75**, 267 (1991).

[7] B. Dhandapani, T. St Clair, and S. T. Oyama, Appl. Catal. A **168**, 219 (1998).

[8] S. Posada-Pérez, F.Viñes, J.A. Rodríguez, and F. Illas, Top. Catal. **58**, 159 (2015).

[9] J. A. Rodriguez and F. Illas, Phys. Chem. Chem. Phys. **14**, 427 (2012)

[10] Y. Liu, T. G. Kelly, J. G. Chen, and W. E. Mustain, ACS Catal. **3**, 1184 (2013).

[11] L. K. Ono and B. Roldán-Cuenya, Catal. Lett. **113**, 8 (2007).

[12] J. A. Rodriguez, P. Liu, F. Viñes, F. Illas, Y. Takahashi and K. Nakamura, Angew. Chem., Int. Ed. **47**, 6685 (2008).

[13] J. A. Rodriguez, P. Liu, Y. Takahashi, K. Nakamura, F. Viñes and F. Illas, J. Am. Chem. Soc. **131**, 8595 (2009).

[14] L. Feria, J. A. Rodriguez, T. Jirsak and F. Illas, J. Catal. **279**, 352 (2011).

[15] J. A. Rodriguez, P. Liu, Y. Takahashi, K. Nakamura, F. Viñes and F. Illas, Top. Catal. **53**, 393 (2010).

[16] J. A. Rodriguez, P. Liu, Y. Takahashi, F. Viñes, L. Feria, E. Florez, K. Nakamura and F. Illas, Catal. Today **166**, 2 (2011).

[17] J. A. Rodriguez, L. Feria, T. Jirsak, Y. Takahashi, K. Nakamura and F. Illas, J. Am. Chem. Soc. **132**, 3177 (2010).

[18] E. Florez, T. Gomez, P. Liu, J. A. Rodriguez and F. Illas, ChemCatChem **2**, 1219 (2010).

[19] J. A. Rodriguez, P. Liu, J. Gomes, K. Nakamura, F. Viñes, C. Sousa and F. Illas, Phys. Rev. B **72**, 075427 (2005).

[20] Y. F. Zhang, F. Viñes, Y. J. Xu, Y. Li, J. Q. Li and F. Illas, J. Phys. Chem. B **110**, 15454 (2006).

[21] F. Viñes, C. Sousa, F. Illas, P. Liu and J. A. Rodriguez, J. Phys. Chem. C **111**, 1307 (2007).

[22] F. Viñes, C. Sousa, F. Illas, P. Liu and J. A. Rodriguez, J. Phys. Chem. C **111** 16982 (2007).

[23] J. A. Rodriguez, P. J. Ramírez, G. G. Asara, F. Viñes, J. Evans, P. Liu, J. M. Ricart, F. Illas, Angew. Chem. Int. Ed. **53**, 11270 (2014).

[24] A. B. Vidal, L. Feria, J. Evans, Y. Takahashi, P. Liu, K. Nakamura, F. Illas and J. A. Rodriguez, J. Phys. Chem. Lett. **3**, 2275 (2012).

[25] J. A. Rodriguez, J. Evans, L. Feria, A. B. Vidal, P. Liu, K. Nakamura, F. Illas, J. Catal. **307**, 162 (2013)

[26] W. Zheng, T. P. Cotter, P. Kaghazchi, T. Jacob, B. Frank, K. Schlichte, W. Zhang, D. S. Su, F. Schüth, and R. Schlögl, J. Am. Chem. Soc. 135, 3458 (2013).

[27] P. Liu and J. A. Rodriguez, J. Phys. Chem. B **110**, 19418 (2006).

[28] M. Patel, M. A. S. Baldanza, V. Teixeira da Silva, and A. V. Bridgwater, App. Catal. A: General **458**, 48 (2013).

[29] *Powder Diffraction File*; JCPDS International Center for Diffraction Data: Pennsylvania, 2004.

[30] J. W. Han, L. W. Li, D. and S. Sholl, J. Phys. Chem. C **115**, 6870 (2011).

[31] J. Ren, C.-F. Huo, J. Wang, Z. Cao, Y.-W. Li, and H. Jiao, Surf. Sci. **600**, 2329 (2006).

[32] H. Tominaga, Y. Aoki, and M. Nagai, Appl. Catal. A **423–424**, 192 (2012).

[33] H. Tominaga and M. Nagai, J. Phys. Chem. B **109**, 20415 (2005).

[34] A. N. Christensen, Acta Chem. Scand. Ser. A **31**, 509 (1977).

[35] T. Wang, Y.W. Li, J. Wang, M. Beller, and H. Jiao, J. Phys. Chem. C **118,** 3162 (2014).

[36] S. Posada-Pérez, F. Viñes, P. J. Ramirez, A. B. Vidal, J. A. Rodriguez, and F. Illas, Phys. Chem. Chem. Phys. **16**, 14912 (2014).

[37] M. D. Porosoff, X. Yang, J. A. Boscoboinik, and J. G. Chen, Angew. Chem., Int. Ed. **53**, 6705 (2014)

[38] H. Tominaga and M. Nagai, Appl. Catal. A **328**, 35 (2007).

[39] A. J. Medford, A. Vojvodic, F. Studt, F. Abild-Pedersen and J. K. Nørskov, J. Catal. **290**, 108 (2012).

[40] C. Pistonesi, M. E. Pronsato, L. Bugyi and A. Juan, J. Phys.Chem. C **116**, 24573 (2012).

[41] T. P. St Clair, S. T. Oyama, D. F. Cox, S. Otani, Y. Ishizawa, R. -L. Lo, K. Fukui, Y. Iwasawa, Surf. Sci. **426**, 187 (1999)

[42] R. L. Lo, K. Fukui, S. Otani, S. T. Oyama, Y. Iwasawa, Jpn. J. Appl. Phys. *38*, 3813 (1999)

[43] K. Jug, B. Zimmermann, P. Calaminici, and A. M. Köster, J. Phys.Chem. **116**, 4497 (2002).

[44] P. Jaque and A. Toro-Labbé, J. Chem. Phys, **17**, 3208 (2002).

[45] J. R. d. S. Politi, F. Viñes, J. A. Rodriguez and F. Illas, Phys. Chem. Chem. Phys., **15**, 12617 (2013).

[46] G. Kresse and J. Furthmuüller, Phys. Rev. B: Condens. Matter Mater. Phys. **54**, 11169 (1996).

[47] J. P. Perdew, K. Burke and M. Ernzerhof, Phys. Rev. Lett., **77**, 3865 (1996).

[48] P. Janthon, S. M. Kozlov, F. Viñes, J. Limtrakul, and F. Illas J. Chem. Theory Comput. **9**, 1631 (2013).

[49] P. Janthon, S. J. Luo, S. M. Kozlov, F. Viñes, J. Limtrakul, D. G. Trulhar and F. Illas J. Chem. Theory Comput. **10**, 3832 (2014).

[50] P. E. Blöchl, Phys. Rev. B: Condens. Matter Mater. Phys, **50**, 17953 (1994).

[51] G. Kresse and D. Joubert, Phys. Rev. B: Condens. Matter Mater. Phys. **59**, 1758 (1999).

[52] H. J. Monkhorst and J. D. Pack, Phys. Rev. B: Solid State **13**, 5188 (1976).

[53] See supplemental material at [URL will be inserted by AIP]

[54] B. Silvi and A. Savin, Nature, **371**, 683 (1994).

[55] R. F. Bader, Atoms in Molecules: A Quantum Theory; Oxford Science: Oxford, U.K., 1990.

[56] P. Calaminici, A. M. Köster, N. Russo, and D. R. Salahub, J. Phys. Chem. **105**, 9546 (1996).

[57] P. Calaminici, M. Pérez-Romero, J. M. Vásquez-Pérez, and A. M. Köster, Comp. Theor. Chem. **1021**, 41 (2013).

[58] E. Florez, W. Tiznado, F. Mondragón, and P. Fuentealba, J. Phys. Chem A, **109**, 7815 (2005).

[59] I. A. Hijazi and Y. H. Park, Eur. Phys. J. D. **59**, 215 (2010).

[60] G. G. Asara, F. Viñes, J. M. Ricart, J. A. Rodriguez, and F. Illas, Surf. Sci. **624**, 32 (2014).

[61] T. Gomez, E. Florez, J. A. Rodriguez, F. Illas, J. Phys.Chem. C **115**, 11666 (2011).

[62] P. B. Balbuena, P. A. Derosa, and J. M. Seminario, J. Phys. Chem. B. **103**, 2830 (1999).

[63] F. Viñes, J. R. B. Gomes and F. Illas Chem. Soc. Rev. **43**, 4922 (2014).

[64] A. Roldan, F. Viñes, F. Illas, J. M. Ricart and K. M. Neyman Theor. Chem. Acc. **120**, 565 (2008).

[65] O. Dulub, M. Batzill, and U. Diebold, Top. Catal. **36**, 65 (2005).

[66] A. Asthagiri, C. Niederberger, A. J. Francis, L. M. Porter, P. A. Salvador, D. S. Sholl, Surf. Sci. **537**, 134 (2003).